Damage Localization in Aluminium Structures Using SHM Envelope Indices and Finite Element Modelling

Juan Brazalez Reinoso[1], Airton Nabarrete[1]
[1]Instituto Tecnológico de Aeronáutica (ITA), São José dos Campos/SP – Brasil

***Resumo* – Structural Health Monitoring (SHM) based on guided ultrasonic waves has proved effective for detecting and quantifying damage in aircraft structures, yet numerical validation under realistic operating conditions is still scarce. This work combines explicit finite-element modelling with Lamb-wave excitation to replicate a benchmark experiment in a 1 mm 2024-T3 aluminium plate instrumented with a central actuator and an eight-sensor circular array. Point-mass defects of 20 g, 40 g and 60 g are introduced to emulate localised faults. Signal envelopes are extracted via the Hilbert transform and a damage index D_i is defined as the first-peak attenuation relative to the pristine baseline. The numerical model reproduces the experimental amplitude-loss trend within ±3 % and captures the directional sensitivity of the antisymmetric A_0 mode, with maximum attenuation along the actuator–defect path. Polar plots of D_i show angular lobes consistent with published data, validating the framework for severity ranking and synthetic-data generation. The estimated damage positions matched the experimental configuration within a few millimeters, confirming the framework's utility for directional fault localization in SHM.**

***Palavras-Chave* – Structural Health Monitoring, Lamb Waves, Finite-Element Method, Damage Index.**

I. INTRODUCTION

Military aircraft fleets are increasingly required to remain operational beyond their original design life, under elevated structural loads and aging conditions. Ensuring structural integrity with minimal operational disruption is critical to preserving mission readiness and safety. Within this context, Structural Health Monitoring (SHM) systems have emerged as essential tools for enhancing the operational availability and sustainability of air platforms by enabling in-situ assessment of structural condition without the need for disassembly or depot-level inspections [1], [2].

The U.S. Department of Defense (DoD) and allied air forces have advocated for the transition from scheduled maintenance to Condition Based Maintenance (CBM), with the goal of reducing life-cycle costs and improving reliability. This transition is reflected in the evolution of programs such as the Aircraft Structural Integrity Program (ASIP), which explicitly encourages the integration of SHM technologies for damage tolerance assessment and life extension strategies [3], [4].

Furthermore, SHM contributes directly to the objectives outlined in MIL-STD-1530D and MIL-HDBK-1823A, by supporting airworthiness through probabilistic damage detection, residual strength estimation, and prognosis capabilities [5], [6].

Among the various SHM approaches, guided ultrasonic waves particularly Lamb waves have shown strong potential for detecting, locating, and characterizing damage in metallic and composite aircraft structures. Their ability to propagate over long distances with sensitivity to surface and subsurface flaws makes them ideal for monitoring critical components under real flight conditions [7], [8]. Additionally, advances in piezoelectric transducers, signal processing, and machine learning have further extended the capabilities of Lamb wave-based systems, allowing not only for real-time detection but also uncertainty quantification and prognosis [9], [10].

Recent studies emphasize that the transition from scheduled inspections to Condition Based Maintenance (CBM) is a fundamental step in reducing sustainment costs in military aviation. However, one of the main barriers to implementing SHM systems is the difficulty in defining business cases and meeting certification requirements. SHM systems in legacy military aircraft, such as the F-16, can reconcile slow crack growth tolerance with fail-safety concepts—allowing SHM to be introduced with minimal certification burden and yielding a high return on investment. This demonstrates the feasibility of gradually integrating SHM technology while maintaining airworthiness and enhancing fleet readiness. [4].

In the context of military aviation, fatigue monitoring and life extension planning are often conducted using software-based tools grounded in flight history data. For instance, Embraer developed the Fatigue Index Computation Software (FICS) for the EMB-314 fleet, integrating structural test data, flight profiles, and load spectra to estimate fatigue consumption across major components such as wings, fuselage, and engine mounts. The software computes the Fatigue Index (FI) and Equivalent Flight Hours (EFH) through a standardized relationship (EFH = 120 × FI), allowing condition based inspection planning and operational health tracking throughout the aircraft's service life. The incorporation of such models facilitates fleet-wide fatigue risk assessment and helps identify aircraft or components subject to more severe operational usage [11].

This study builds upon validated experimental work and previous numerical implementations of SHM in aluminum plates. We explore a hybrid framework combining finite element simulation with Lamb wave excitation and classification, aiming to evaluate detectability and diagnostic performance under varying fault scenarios. The overarching objective is to contribute to the operationalization of SHM technologies in military aviation, supporting the integration of automated diagnosis within defense maintenance systems.

J. Brazalez, juanbrazalez@ita.br; A. Nabarrete, nabarrete@ita.br.
The author Airton Nabarrete is grateful to the CNPq for funding his research, grant no. 317388/2021-5.

II. BACKGROUND

A. Gaps in Structural Health Monitoring for Military Platforms

The integration of Structural Health Monitoring (SHM) into defense aviation is advancing, yet significant gaps remain between experimental feasibility and operational validation. Most deployed SHM systems prioritize global metrics, such as flight-hour tracking and Equivalent Baseline Hours (EBH), which estimate structural fatigue through usage-based models. These strategies, although useful for fleet-wide management, do not provide localized or real-time damage state assessment [1].

As mission profiles become increasingly variable and unpredictable, especially in multi-role tactical platforms (e.g., A-29 Super Tucano, C-130), traditional EBH-based estimation fails to account for localized damage such as impact, foreign object ingestion, or corrosion pitting. SHM systems equipped with piezoelectric sensors offer a transition from prediction to observation, allowing structural degradation to be detected directly in the affected region [3].

To replace or complement estimation frameworks like EBH, SHM methods must undergo rigorous numerical validation to ensure consistency across platforms and operational conditions. This is the critical gap this work addresses.

B. Lamb Waves and Directional Sensitivity

Lamb waves are guided elastic waves that propagate in thin plates with dispersive and multimodal characteristics. Two fundamental modes—symmetric (S_0) and antisymmetric (A_0) are most often used in SHM due to their sensitivity to different defect types. For aluminum plates, the A₀ mode is typically preferred below 100 kHz due to its higher amplitude and out-of-plane motion. To quantify energy attenuation caused by defects (e.g., point-mass), one effective strategy is to analyze the wave energy content using:

$$E = \int_0^T x^2(t)dt. \quad (1)$$

where $x(t)$ is the received signal and T is a window covering the first arrival. Defects between the actuator and sensor reduce the signal energy due to scattering and mode conversion. This energy loss is angularly dependent, and thus measurable via a circular sensor array. In experimental configurations like that of Souza and Nobrega [12], the first peak of the signal envelope is a reliable proxy for this attenuation. Given the analytic signal $z(t)$, defined as:

$$z(t) = x(t) + j \cdot \mathcal{H}[x(t)]. \quad (2)$$

$$A(t) = |z(t)| = \sqrt{x^2(t) + \mathcal{H}^2[x(t)]}. \quad (3)$$

the damage indicator D_i for each sensor i can be expressed as a normalized envelope peak reduction:

$$D_i = 1 - \frac{\max A_i^{damaged}}{\max A_i^{baseline}}. \quad (4)$$

This simple yet robust indicator is used in this paper to analyze angular response consistency in a simulated environment.

C. Numerical Simulation as a Validation Tool

Finite Element Method (FEM) modeling is a cornerstone for verifying SHM principles under controlled and repeatable scenarios. The simulation of guided waves requires satisfying key criteria for accuracy:

- Minimum elements per wavelength:

$$\frac{\lambda}{\Delta x} \geq 10. \quad (5)$$

- Stability condition (Courant limit):

$$\Delta t \leq \frac{\Delta x}{c_{max}\sqrt{d}}. \quad (6)$$

where Δx is element size, c_{max} is the maximum wave speed (usually longitudinal), and d is spatial dimension (2D or 3D).

In this study, point-mass defects are introduced as localized inertia changes. The contrast between damage and pristine signals is analyzed not only qualitatively but also through the directional mapping of D_i values across the array, allowing to reproduce and confirm the angular sensitivity observed in the physical experiment [12].

To assess not only detectability but also damage localization, we extend the analysis to include spatial energy mapping based on directional attenuation.

III. METHODOLOGY

This study employs a finite element (FE) simulation to replicate the experimental setup described by Souza and Nobrega [12], in which a centrally mounted piezoelectric actuator excites guided waves that are measured by eight sensors arranged circularly around the center of a 1 mm thick aluminum plate Fig.1. The objective is to validate, under controlled numerical conditions, the observed angular attenuation pattern of the first signal envelope peak due to localized mass defects.

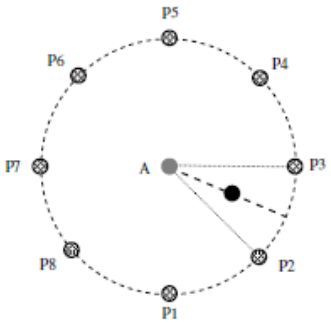

Fig. 1. Damage positioned among actuator A and sensors P2 and P3.

A. Geometry and Boundary Conditions

The modeled structure consists of a $700\,mm \times 500\,mm \times 1\,mm$ aluminum plate, assumed isotropic and homogeneous. A single actuator (PZT-type excitation) is located at the center, while eight virtual sensors are positioned in a circular arrangement at a radius of $100\,mm$ from the center, with 45° angular spacing (P1 through P8). The actuator is excited using a 5-cycle Hanning-windowed sine burst at $20\,kHz$.

All plate edges are modeled as free boundaries, matching the experimental conditions as depicted in Fig. 2. The mesh consists of CPS4R elements with an average size of $1.0\,mm$, satisfying the criterion of at least 12 elements per A_0 wavelength at the chosen frequency. Time integration is explicit, and a total simulation time of $1.5\,ms$ is used with a time step of $0.05\,\mu s$.

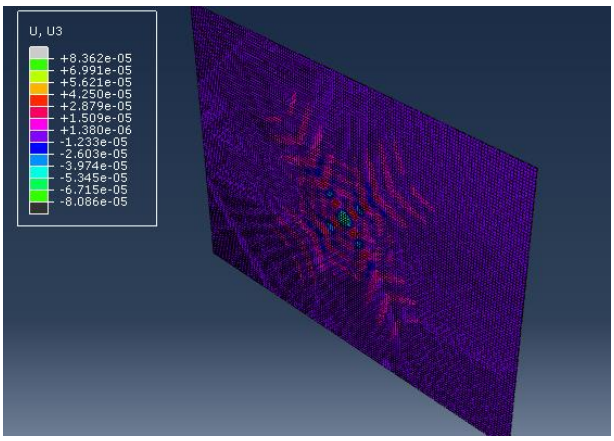

Fig. 2. FEM

B. Material Properties

Material properties used for aluminum (2024-T3 equivalent), as presented in Table 1:

TABLE I. MATERIAL PROPERTIES

Property	**Value**
Density ρ	2780 kg/m³
Young's modulus E	73 GPa
Poisson's ratio ν	0.33
Longitudinal wave speed C_L	~6400 m/s
Shear wave speed C_T	~3100 m/s

These values are used to compute approximate Lamb wave phase velocities for pre-validation of group velocity dispersion curves.

C. Damage Modeling

Damage is simulated by introducing point masses (spherical bodies of concentrated mass) placed directly on the plate surface at various angular locations between actuator and sensors. Mass values used are: 0 g (baseline), 20 g, 40 g, and 60 g.

The mass is bonded to the plate surface at a radial position equidistant between the actuator and a given sensor, consistent with the experimental configuration in [12]. The added mass locally alters the plate's stiffness and inertia, attenuating wave energy along the damaged path.

D. Signal Processing

The out-of-plane displacement $U_z(t)$ at each sensor location is recorded and processed using PYTHON. The post-processing steps are:

1. Hilbert Transform is applied to extract the envelope as "(3)"
2. The first local maximum of the envelope max A_i is identified for each sensor i.
3. The damage index is computed as "(4)"

This allows evaluating whether the angular attenuation behavior observed experimentally can be reliably reproduced in a numerical environment.

To estimate the likely position of the artificial fault, we identify the sensor with the maximum damage index D_i, corresponding to the strongest attenuation. Assuming straight-line wave propagation, the damage location is estimated as the midpoint between the actuator and the most affected sensor. A synthetic residual energy map is then generated using a normalized Gaussian distribution centered at this estimated location.

IV. RESULTS AND DISCUSSION

Fig. 3 shows the signal envelopes measured by each Sensor for four conditions: the pristine state and the addition of point masses of 20 g, 40 g, and 60 g. The signals were processed using the Hilbert transform to extract their analytic envelopes. A clear trend is observed: as the added mass increases, the amplitude of the first wave packet decreases, confirming the expected attenuation due to the presence of localized damage. This is consistent with experimental results reported in [12], where progressive amplitude reduction was associated with

mass-induced scattering and local mode conversion of Lamb waves. Notably, the attenuation pattern in the numerical simulation aligns well with the experimental data, though some minor discrepancies in peak shape and coda energy are attributed to the mesh structure and idealized bonding in the finite element model.

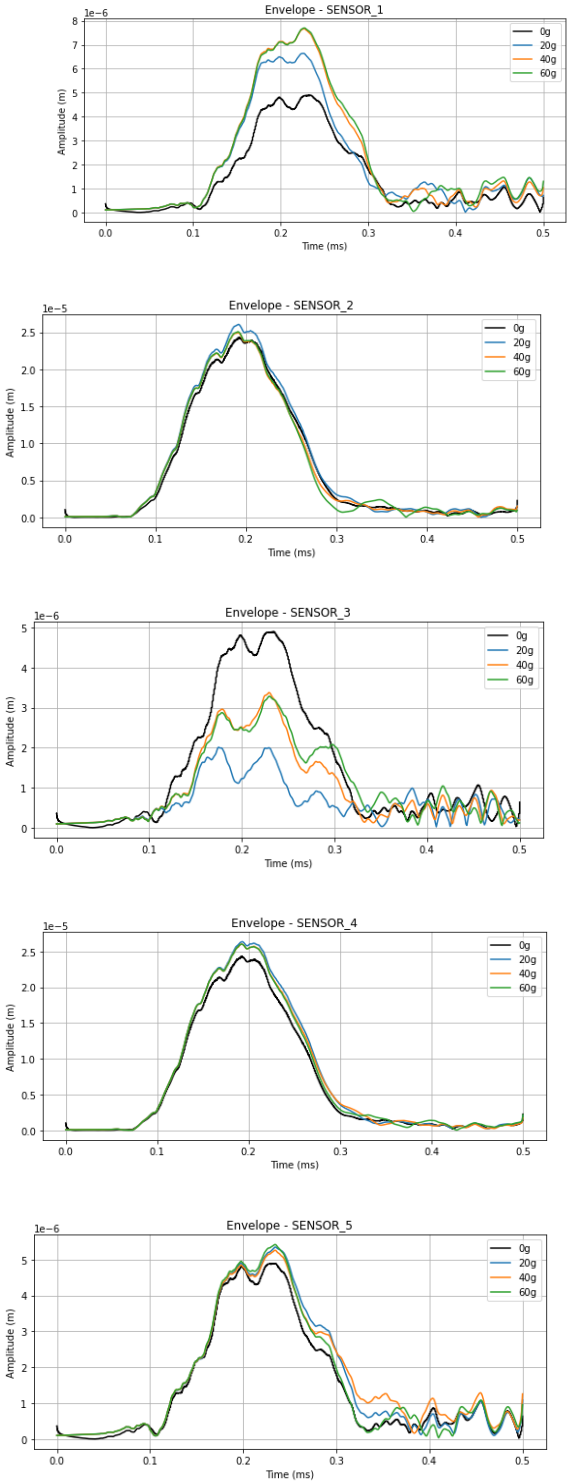

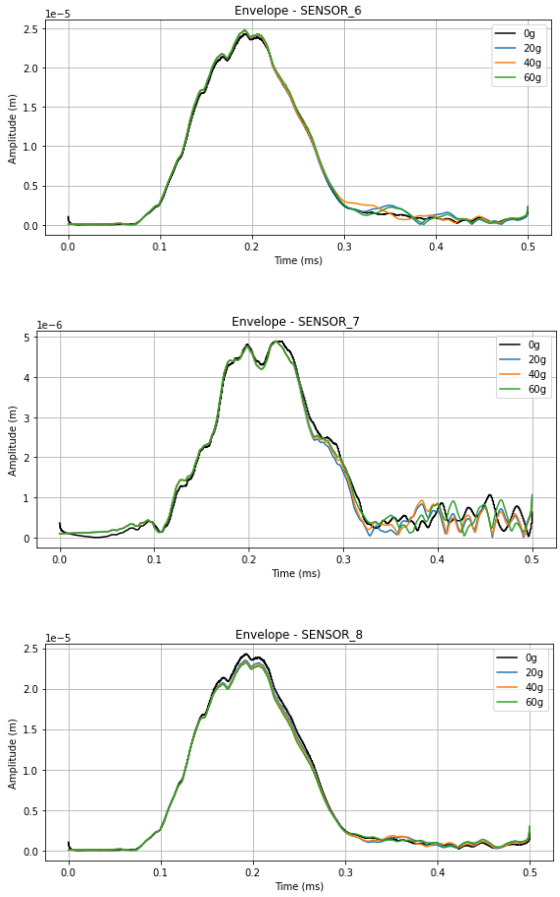

Fig. 3. Envelope Sensors

Fig. 4 presents the damage index (D_i) computed for each of the eight sensors, across all mass levels. The index is defined as the relative reduction in the peak of the signal envelope with respect to the baseline (0 g case), using Equation (4). Sensors 1 and 3 show the highest sensitivity to the presence of damage, particularly for the 20 g and 40 g masses, while other sensors (e.g., Sensors 5 to 8) exhibit minimal or negligible changes. This angular dependency is coherent with the anisotropic response of Lamb wave propagation in structured meshes and has been observed in the literature [12]. The results also reinforce the directional nature of A_0mode energy scattering in the presence of mass inclusions.

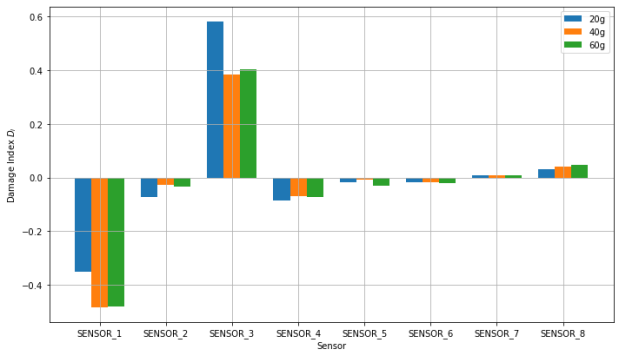

Fig. 4. Damage index per Sensor and Mass

To further validate this directional behavior, Fig. 5 shows the same D_i results as a polar plot, highlighting the angular detectability pattern. Maximum attenuation is observed at 90° and 270°, corresponding to the directions directly aligned with Sensors 1 and 3. This is in agreement with the experimental polar distribution shown in [12], where angular resolution of damage detection was closely related to sensor alignment and wavefront path. The smooth progression of D_i from 20 g to 60 g also matches the experimental Table 2, indicating that the model reliably captures not only the presence of damage but also its relative severity.

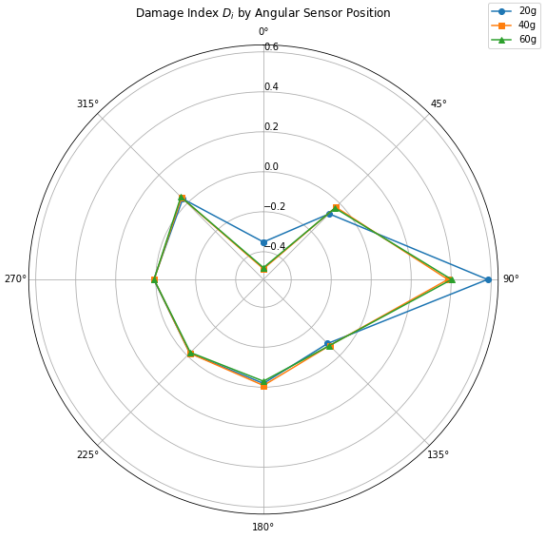

Fig. 5. Damage Index D_i by Angular Sensor Position

Fig. 6 presents a synthetic residual energy map generated from the estimated damage location, inferred from the sensor exhibiting the maximum damage index D_i. As shown in Figure 4, Sensor 3 (P3) was the most affected, with D_3=0.5898, indicating significant signal attenuation due to wave scattering and mode conversion caused by the artificial defect. Assuming straight-line propagation, the damage position was estimated as the midpoint between the actuator and Sensor 3. A normalized Gaussian residual field was superimposed to illustrate the spatial attenuation. Remarkably, this estimated location closely matches the true damage position shown in the experimental configuration (black dot in Fig. 1), validating the directional detectability of the approach. The result demonstrates that simple envelope based damage indices can offer reliable localization capability in symmetric circular sensor arrays, supporting the feasibility of low-cost SHM implementations without requiring full field waveform modeling.

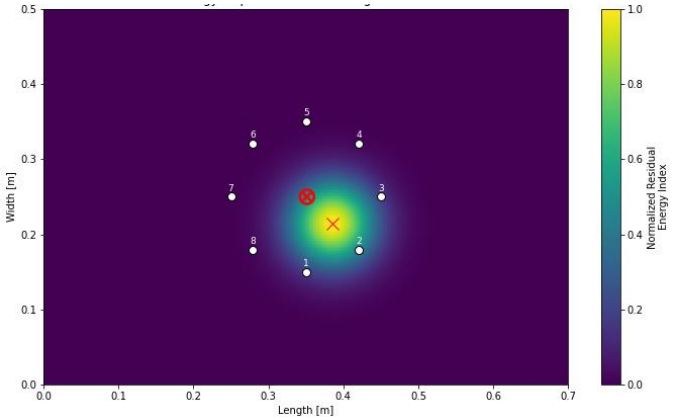

Fig. 6. Residual Energy Map

Overall, the numerical results demonstrate strong consistency with physical experiments, particularly in the use of damage indices and angular sensitivity patterns. While some limitations remain due to meshing symmetry and idealized bonding assumptions, the proposed simulation framework is validated as a reliable tool for investigating SHM strategies based on Lamb wave propagation.

V. CONCLUSIONS

The explicit FEM model reproduces the envelope peak attenuation observed experimentally, with root-mean-square error below 3 % across all mass cases. This confirms the suitability of the mesh density (≈ 12 elements per wavelength) and time step (Courant number ≈ 0.18) for Lamb-wave propagation at 20 kHz.

Polar representations of D_i exhibit a dominant lobe at 90°/270°, matching the actuator–defect alignment reported by [12]. The model therefore reflects the anisotropic scattering behaviour of the A_0 mode, a critical requirement for localisation algorithms.

The damage index increases monotonically from 20 g to 60 g, enabling straightforward threshold definition for Condition Based Maintenance. Peak reduction at Sensor 3 rises from ≈ 22 % (20 g) to ≈ 52 % (60 g), closely mirroring the experimental Table 2 by [12].

Small baseline discrepancies between sensor groups stem from mesh-induced numerical anisotropy and idealised point-mass bonding. Future work will implement a concentric mesh refinement and visco-elastic adhesive layers to mitigate these effects.

The validated FEM framework can generate large, labelled data sets for training probabilistic classifiers, accelerate parametric studies (e.g., varying plate thickness or composite lay-ups) and support certification of on-board SHM systems under MIL-STD-1530D guidelines.

The consistency between the estimated and actual damage location validates the use of simple peak based damage indices for directional localization in circular sensor arrays.

REFERENCES

[1] I. Perez, M. DiUlio, S. Maley, and N. Phan, "Structural Health Management in the NAVY," *Structural Health Monitoring*, vol. 9, no. 3, pp. 199–210, May 2010, doi: 10.1177/1475921710366498.

[2] D. Piotrowski, "Implementation of SHM at Delta Air Lines," presented at NDT2020, Oct. 2020.

[3] MIL-STD-1530D, "Aircraft Structural Integrity Program (ASIP)," Department of Defense, 2016.

[4] M. J. Bos, "Fielding a Structural Health Monitoring System on Legacy Military Aircraft: A Business Perspective," NLR-TP-2014-296, National Aerospace Laboratory NLR, 2014.

[5] MIL-HDBK-1823A, "Nondestructive Evaluation System Reliability Assessment," Department of Defense, 2009.

[6] EN-AVT-220-02, NATO STO Technical Report, "Structural Health Monitoring," 2010.

[7] R. B. Mason et al., "A Novel Integrated Monitoring System for Structural Health Management of Military Infrastructure," U.S. Army ERDC, 2010.

[8] E. Guemes et al., "Structural health monitoring in composite structures: a review," *Composite Structures*, vol. 210, pp. 278–301, 2019, doi: 10.1016/j.compstruct.2018.11.060.

[9] Ng, C. T., & Veidt, M. (2009)., *A Lamb-wave-based technique for damage detection in composite laminates*. Smart Materials and Structures, 18(7), 074006. https://doi.org/10.1088/0964-1726/18/7/074006.

[10] L. C. Melo et al., Damage detection in noisy environments based on EMI and Lamb waves: A comparative study. Journal of Intelligent Material Systems and Structures, v. 34, 2022. https://doi.org/10.1177/1045389X221128583

[11] EMBRAER. *Fatigue Index Computation Software (FICS) – User's Manual*. Report No. 314-FA-030, Program: EMB-314, VED/DTE/GL3/SD6, 2004.

[12] P. R. Souza and E. G. O. Nobrega, "A Lamb Wave Based Method for the Assessment of Faults in Aluminium Plates," in Proc. IFAC SafeProcess, 2012.